Electronic-Structure-Driven Magnetic Ordering in a Kondo Semiconductor $CeOs_2Al_{10}$

Shin-ichi Kimura,[1,2,*] Takuya Iizuka,[2] Hidetoshi Miyazaki,[1] Akinori Irizawa,[3,†] Yuji Muro,[4] and Toshiro Takabatake[4,5]

[1]*UVSOR Facility, Institute for Molecular Science, Okazaki 444-8585, Japan*
[2]*School of Physical Sciences, The Graduate University for Advanced Studies (SOKENDAI), Okazaki 444-8585, Japan*
[3]*Graduate School of Science and Technology, Kobe University, Nada-ku, Kobe 657-8501, Japan*
[4]*Department of Quantum Matter, ADSM, Hiroshima University, Higashi-Hiroshima, Hiroshima 739-8530, Japan*
[5]*Institute for Advanced Materials Research, Hiroshima University, Higashi-Hiroshima, Hiroshima 739-8530, Japan*

(Received 20 May 2010; published 4 February 2011)

We report the anisotropic changes in the electronic structure of a Kondo semiconductor $CeOs_2Al_{10}$ across an anomalous antiferromagnetic ordering temperature (T_0) of 29 K, using optical conductivity spectra. The spectra along the a and c axes indicate that an energy gap due to the hybridization between conduction bands and nearly local $4f$ states, namely the c-f hybridization gap, emerges from a higher temperature continuously across T_0. Along the b axis, on the other hand, another energy gap with a peak at 20 meV becomes visible at 39 K ($> T_0$) and fully opens at T_0 because of a charge instability. This result implies that the appearance of the energy gap, as well as the change in the electronic structure along the b axis, induces the antiferromagnetic ordering below T_0.

DOI: 10.1103/PhysRevLett.106.056404 PACS numbers: 71.27.+a, 78.20.−e

Rare-earth intermetallic compounds provide useful materials with characteristic physical properties, such as heavy fermions, Kondo semiconductors or insulators, and so on, due to the interaction between the local $4f$ electrons and the conduction electrons, namely c-f hybridization [1]. With regard to these properties, Kondo semiconductors are known to have a c-f hybridization gap on the Fermi level (E_F), even though the magnetic susceptibility at high temperature obeys the Curie-Weiss law, indicating the local $4f$ character [2]. Typical Kondo semiconductors such as SmB_6, YbB_{12}, $Ce_3Bi_4Pt_3$, CeRhSb, and others studied previously have no phase transition below the Kondo temperature (T_K) because the magnetic moments of Ce $4f$ are quenched due to the Kondo singlet state via strong c-f hybridization.

However, the recently discovered Kondo semiconductors CeM_2Al_{10} (M = Os, Ru), which forms an orthorhombic $YbFe_2Al_{10}$ type crystal structure (space group $Cmcm$, No. 63) [3], show an anomalous phase transition at a characteristic temperature T_0 (28.7 K for M = Os, 27.3 K for Ru) below the Kondo temperature ($T_K \sim$ 100 K for Os, 60 K for Ru) [4–6]. This is in contrast to the related material $CeFe_2Al_{10}$, which is a typical Kondo semiconductor without any phase transition even at very low temperatures [7,8]. The electrical resistivities of $CeOs_2Al_{10}$ and $CeRu_2Al_{10}$ commonly show a positive jump at T_0. However, $CeOs_2Al_{10}$ shows a semiconducting activation-type electrical resistivity different from that above T_0, despite the fact that $CeRu_2Al_{10}$ has metallic characteristics below T_0 [9,10]. Very recently, below T_0, long-range antiferromagnetic ordering with small magnetic moments has been observed in both $CeOs_2Al_{10}$ and $CeRu_2Al_{10}$ [11–13]. Since the Ce-Ce distance is about 5 Å, which is longer than that of normal Ce compounds, however, the Ruderman-Kittel-Kasuya-Yoshida (RKKY) interaction is not believed to be the origin of the phase transition at T_0. So far, some explanations for the antiferromagnetic ordering have been proposed [5,6,14,15], but its origin remains unknown.

In this Letter, we describe an investigation into the origin of the anomalous phase transition at T_0, as well as the change in the electronic structure of $CeOs_2Al_{10}$, using temperature-dependent polarized optical conductivity [$\sigma(\omega)$] spectra. At higher temperatures, $CeOs_2Al_{10}$ has the electronic structure of an anisotropic semiconductor. Below about 39 K, which is higher than T_0, on the other hand, a pronounced peak structure of the $\sigma(\omega)$ spectra only along the b axis appears at a photon energy $\hbar\omega$ of 20 meV despite the fact that the $\sigma(\omega)$ spectra along the a- and c axes are unchanged except for a reduction in thermal broadening. The spectral shape and the evolution of the energy gap imply that the energy gap originates from a charge instability as well as a change-density wave (CDW) due to structural distortion observed by electron diffraction [9]. The energy gap along the b axis fully opens below T_0. This result indicates that opening of the energy gap, as well as the change in electronic structure due to the charge instability, induces the anomalous antiferromagnetic ordering at T_0.

Near-normal incident polarized optical reflectivity [$R(\omega)$] spectra were acquired in a very wide photon-energy region of 2 meV—30 eV to ensure an accurate Kramers-Kronig analysis (KKA). Single-crystalline $CeOs_2Al_{10}$ was synthesized by the Al-flux method [9] and was well-polished using 0.3 μm grain-size Al_2O_3 lapping film sheets for the $R(\omega)$ measurements. Martin-Puplett and Michelson type rapid-scan Fourier spectrometers (JASCO Co. Ltd., FARIS-1 and FTIR610) were used at photon energies $\hbar\omega$ of 2–30 meV and 5 meV–1.5 eV, respectively,

with a specially designed feedback positioning system to maintain the overall uncertainty level less than ±0.5% at sample temperatures T in the range of 8–300 K [16]. To obtain the absolute $R(\omega)$ values, the samples were evaporated *in-situ* with gold, whose spectrum was then measured as a reference. At $T = 300$ K, $R(\omega)$ was measured for energies 1.2–30 eV by using synchrotron radiation [17]. In order to obtain $\sigma(\omega)$ via KKA of $R(\omega)$, the spectra were extrapolated below 2 meV with a Hagen-Rubens function, and above 30 eV with a free-electron approximation $R(\omega) \propto \omega^{-4}$ [18].

The $R(\omega)$ spectra obtained along the a axis ($E \parallel a$), b axis ($E \parallel b$), and c axis ($E \parallel c$) are shown in Fig. 1. As can be seen in the inset, the $R(\omega)$ spectra monotonically decrease up to $\hbar\omega = 10$ eV because the conduction band of Al expands to about 10 eV below E_F according to the band calculation (not shown). The characteristic double-peak structure of Ce compounds in the energy range of 100–300 meV, which originates from the top of the valence band to the unoccupied Ce $4f$ state with spin-orbit splitting [19], slightly appears only in $E \parallel b$. In addition, the x-ray photoemission spectrum of the Ce $3d$ core level suggests mixed valence of the Ce ion (not shown) [20]. Both of these features indicate strong c-f hybridization intensity.

Let us focus on the spectra below 100 meV. There are two sharp peaks in $E \parallel a$, one peak in $E \parallel b$, and three peaks in $E \parallel c$ in the range $\hbar\omega = 10$–25 meV due to optical phonons. Except for these peaks, the $R(\omega)$ spectra for all principal axes at 300 K are Drude-like spectra that increase to unity with decreasing photon energy, indicating a metallic character. Below 80 K, the value of $R(\omega)$ below 50 meV rapidly decreases on cooling, and eventually, at the lowest accessible photon energy, $R(\omega)$ does not close to unity at 8 K except for $E \parallel b$. This indicates the existence of an energy gap; i.e., the material changes to an insulator. This result is consistent with the electrical resistivity [9].

The temperature-dependent $\sigma(\omega)$ spectra derived from KKA of the $R(\omega)$ spectra in Fig. 1 are shown in Fig. 2. The $\sigma(\omega)$ spectra for all principal axes at 300 K monotonically increase with decreasing photon energy, again indicating a metallic character. Commonly in all principal axes, the $\sigma(\omega)$ intensity below $\hbar\omega = 60$ meV decreases on cooling, and at 80 K, a broad shoulder structure appears at about 45 meV, which indicates the energy gap due to the strong c-f hybridization similar to other Kondo semiconductors [21–24].

In $E \parallel a$ and $E \parallel c$, the gentle shoulder structures at about 50 meV at 80 K gradually evolve below 130 K and an energy-gap structure appears at the low-energy side of the peak as the temperature decreases to the minimum. However, the gap shape and energy do not change with temperature (except for the reduction in thermal broadening), unlike the case in $E \parallel b$. Below 40 K, a sharp Drude structure appears below 10 meV that differs from the spectral shape above 80 K. Therefore, the gap structure drastically changes near T_0. At 8 K, the Drude structure disappears in the spectral range and a clear energy gap opens, despite the fact that the direct current conductivity along the a axis is about 4000 to 3000 $\Omega^{-1}\,\mathrm{cm}^{-1}$ in all temperature regions. This means that a very narrow Drude peak due to in-gap states must appear below the

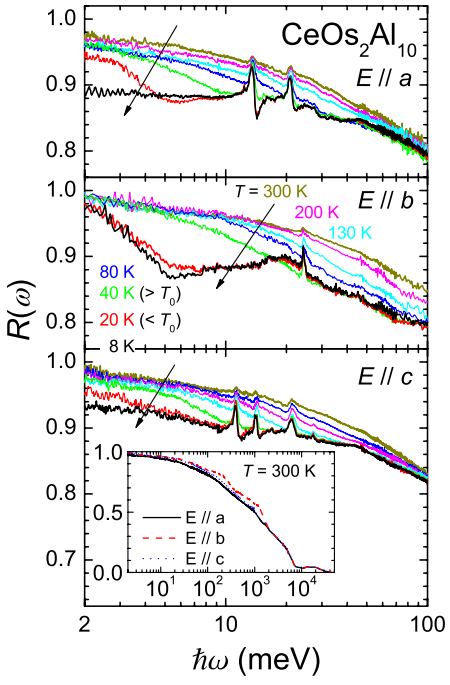

FIG. 1 (color online). Low-energy portion of the temperature-dependent polarized reflectivity [$R(\omega)$] spectra of $CeOs_2Al_{10}$ along three principal axes. (Inset) The entire reflectivity spectra at 300 K along the a axis (solid lines), b axis (dashed lines), and c axis (dotted lines).

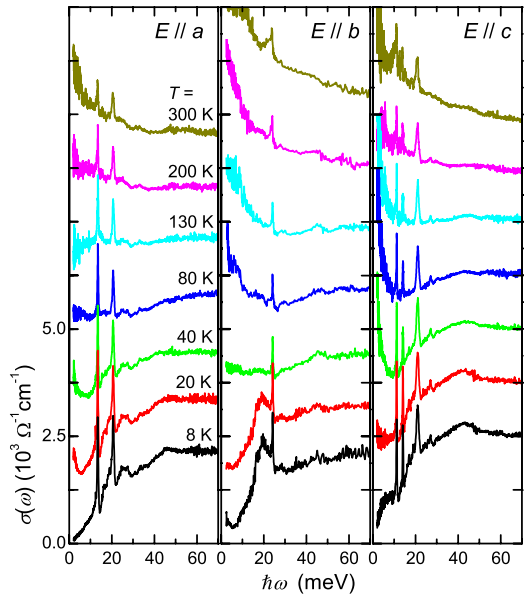

FIG. 2 (color online). Temperature-dependent polarized optical conductivity [$\sigma(\omega)$] spectra of $CeOs_2Al_{10}$ in the photon-energy region below 70 meV. Each of the lines is shifted by $1.25 \times 10^3\ \Omega^{-1}\,\mathrm{cm}^{-1}$ for clarity.

accessible energy region. The origin of the in-gap states is not clear at present.

In $E \parallel b$, the overall temperature dependence is similar to those in $E \parallel a$ and $E \parallel c$, but one peak at and an energy gap below 20 meV suddenly appear at temperatures between 20 and 40 K. To assist in studying the spectral change in detail, Figs. 3(a)–3(c) show the fine temperature dependence ($\Delta T = 2$ K) of the $\sigma(\omega)$ spectra at temperatures from 10 to 40 K in the three principal axes. With decreasing temperature, the spectral weight below 10 meV decreases in $E \parallel a$ and $E \parallel c$. The temperature dependence of the $\sigma(\omega)$ intensity at 5 meV is plotted as σ_a(5 meV) for $E \parallel a$ and σ_c(5 meV) for $E \parallel c$ in Fig. 3(d). Both σ_a(5 meV) and σ_c(5 meV) monotonically decrease with decreasing temperature and do not show anomalies at T_0. The temperature dependence is the same as that of typical Kondo semiconductors [21–24]; i.e., the state in $E \parallel a$ and $E \parallel c$ can be regarded as that of a Kondo semiconductor.

In $E \parallel b$, on the other hand, not only does the spectral weight below 10 meV decrease, but also a peak grows at 20 meV with decreasing temperature. As seen in the σ_b(5 meV) and σ_b(20 meV) behavior, the spectral weight shifts from the lower to the higher energy side across the energy gap. The change starts at about 39 K (hereafter, T^*), not T_0. T^* is the temperature of maximum magnetic susceptibility (M/H) and of the upturn in electrical resistivity (ρ) [9]. Therefore, the downturn in M/H and upturn in ρ originate from generation of the 20-meV peak. In addition, the drastic change in the electronic structure in $E \parallel b$ is consistent with the finding that the temperature-dependent ρ in $E \parallel b$ at around T^* is the largest among those of all the principal axes.

To clarify the difference in temperature dependence of the $\sigma(\omega)$ spectra in $E \parallel b$, the ratio $[\sigma(\omega, T)/\sigma(\omega, 40\ \mathrm{K})]$ spectra, i.e., $\sigma(\omega)$ at a given temperature divided by that at 40 K, are shown in Fig. 4(a). These plots clearly demonstrate the transfer of the spectral weight across T_0 and T^*. In the figure, a peak that appears at 20 meV at 10 K shifts to the low-energy side and broadens with increasing temperature. From the temperature-dependent peak structure, the peak energy, the energy at the half-peak intensity (midpoint), and the onset of the gap that is the linear extrapolation of the slope to zero after subtracting the residual conductivity due to carriers [indicated by the horizontal dashed line in Fig. 4(a)] are plotted as a function of temperature in Fig. 4(b). The peak, midpoint, and onset correspond to energy levels at the density of states near E_F, as shown in the inset in Fig. 4(a). In the same way as in Fig. 3(d), the peak is generated below T^* and does not have an anomaly at T_0. However, the onset becomes visible below T_0. These results imply that the electronic structure is modulated below T^* and the energy gap fully opens below T_0. At T_0, antiferromagnetic ordering is developed. This indicates that the magnetic phase transition is driven by the electronic structure as well as the energy gap opening in $E \parallel b$. The energy of the midpoint, indicated by the solid circles in Fig. 4(b), develops below a slightly higher temperature than T_0. The temperature dependence of

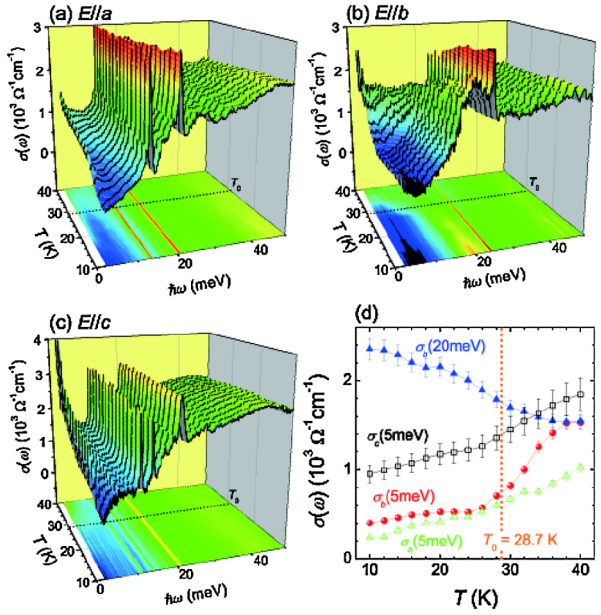

FIG. 3 (color online). Temperature-dependent optical conductivity $[\sigma(\omega)]$ spectra in $E \parallel a$ (a), $E \parallel b$ (b), and $E \parallel c$ (c) at temperatures from 10 to 40 K. (d) Temperature dependence of representatives of spectral change. σ_x(5 meV) [$x = a, b, c$ (x is axis name)] and σ_b(20 meV) are the intensities of the $\sigma(\omega)$ spectra at 5 and 20 meV, respectively.

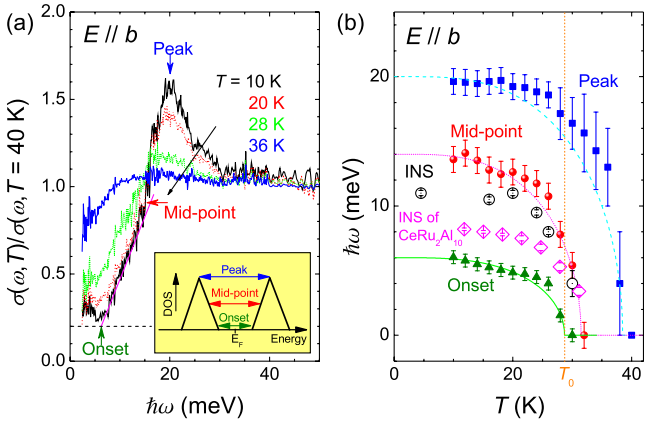

FIG. 4 (color online). (a) Ratio spectra of optical conductivity $[\sigma(\omega)]$ at 10, 20, 28, and 36 K, derived from that at 40 K along the b axis. The residual conductivity is indicated by the horizontal dashed line. (Inset) Expected density of states (DOS) near E_F and corresponding energy levels of "Peak", "Midpoint", and "Onset" in $\sigma(\omega, T)/\sigma(\omega, T = 40\ \mathrm{K})$ spectra. (b) Temperature dependence of the peak energy (solid squares), the energy at the midpoint (solid circles), and the onset (solid triangles) indicated in (a). The inelastic neutron peaks of $CeOs_2Al_{10}$ (open circles, Ref. [12]) and of $CeRu_2Al_{10}$ (open diamonds, Ref. [13]) in which the temperature is normalized against T_0 are also plotted. The solid, dotted, and dashed lines are the temperature-dependent energy gaps predicted by BCS theory with $T_c = 28.7$ K (T_0), 31 K, and 39 K (T^*), respectively.

the midpoint is meaningfully consistent with the peak of inelastic neutron scattering (INS) of the same material and the related material $CeRu_2Al_{10}$ with the temperature normalized by T_0 [12,13]. In the figure, the temperature dependence of the superconducting gap predicted by BCS theory is also plotted for reference. The temperature dependence at all data points is similar to, but deviates slightly from, the BCS curves. This result is consistent with the previous study of CDW and spin-density wave (SDW) transitions such as that of $(TMTSF)_2PF_6$ [25]. In the case of $CeOs_2Al_{10}$, no magnetic transition was observed at T^*. Therefore, CDW is more plausible for the origin of T^*. This is consistent with the observed superlattice reflections along the $[0\bar{1}1]$ direction by electron diffraction [9].

The change in the $\sigma(\omega)$ spectrum due to the CDW and SDW transitions has previously been studied experimentally in $1T$-$TiSe_2$ [26], $P_4W_{14}O_{50}$ [27], $(TMTSF)_2PF_6$ [25], Cr [28], and others. In all cases, the data obtained have indicated that the peak energy (E_{peak}) is significantly larger than the mean-field BCS value of $3.52k_BT_c$, where T_c is the critical temperature. In the case of $CeOs_2Al_{10}$, the CDW transition temperature T_c can be regarded as T^*. Because E_{peak} at 10 K is 20 ± 1.2 meV ($\sim 250 \pm 15$ K), the peak energy is about $(6.4 \pm 0.4)k_BT^*$. This is consistent with the results of previous studies on CDW/SDW gaps, for instance $E_{peak} = 9.0k_BT_c$ in $(TMTSF)_2PF_6$ [25] and $E_{peak} = 6.0k_BT_c$ in Cr [28]. Therefore, the CDW scenario is again supported.

To summarize, the electronic structure and origin of the anomalous phase transition of $CeOs_2Al_{10}$ were investigated by the measurement of temperature-dependent polarized optical conductivity spectra. Along the a and c axes, the spectral weight at energies lower than 10 meV monotonically decreased on cooling, indicating a Kondo semiconductor characteristic with an energy gap of about 10 meV realized in all temperatures. In contrast, along the b axis, a CDW energy gap opened below 39 K, which is higher than T_0, and the onset of the energy gap become visible at T_0. Therefore, the anomalous antiferromagnetic transition at T_0 is concluded to be driven by CDW transition along the b axis, in contrast to the lack of phase transition along the a and c axes.

We would like to thank Mr. Hajiri for his help of Ce $3d$ XPS measurement. Part of this work was supported by the Use-of-UVSOR Facility Program (BL7B, 2009) of the Institute for Molecular Science. The work was partly supported by a Grant-in-Aid for Scientific Research from MEXT of Japan (Grant No. 22340107, 20102004).

*kimura@ims.ac.jp

†Present address: The Institute of Scientific and Industrial Research, Osaka University, Ibaraki, Osaka 567-0047, Japan.

[1] A. C. Hewson, *The Kondo Problem to Heavy Fermions* (Cambridge University Press, Cambridge, England, 1993).
[2] T. Takabatake *et al.*, J. Magn. Magn. Mater. **177–181**, 277 (1998), and references therein.
[3] V. M. T. Thiede, T. Ebel, and W. Jeitschko, J. Mater. Chem. **8**, 125 (1998).
[4] A. M. Strydom, Physica (Amsterdam) **404B**, 2981 (2009).
[5] T. Nishioka *et al.*, J. Phys. Soc. Jpn. **78**, 123705 (2009).
[6] M. Matsumura *et al.*, J. Phys. Soc. Jpn. **78**, 123713 (2009).
[7] Y. Muro *et al.*, J. Phys. Soc. Jpn. **78**, 083707 (2009).
[8] Y. Muro *et al.*, J. Phys. Conf. Ser. **200**, 012136 (2010).
[9] Y. Muro *et al.*, Phys. Rev. B **81**, 214401 (2010).
[10] T. Takesaka *et al.*, J. Phys. Conf. Ser. **200**, 012201 (2010).
[11] D. D. Khalyavin *et al.*, Phys. Rev. B **82**, 100405(R) (2010).
[12] D. T. Adroja *et al.*, Phys. Rev. B **82**, 104405 (2010).
[13] J. Robert *et al.*, Phys. Rev. B **82**, 100404(R) (2010).
[14] K. Hanzawa, J. Phys. Soc. Jpn. **79**, 043710 (2010).
[15] H. Tanida *et al.*, J. Phys. Soc. Jpn. **79**, 063709 (2010).
[16] S. Kimura, JASCO Report **50**, 6 (2008). [in Japanese]
[17] K. Fukui *et al.*, Nucl. Instrum. Methods Phys. Res., Sect. A **467–468**, 601 (2001).
[18] M. Dressel and G. Grüner, *Electrodynamics of Solids* (Cambridge University Press, Cambridge, England, 2002).
[19] S. Kimura, T. Iizuka, and Y. S. Kwon, J. Phys. Soc. Jpn. **78**, 013710 (2009).
[20] H. Miyazaki, T. Hajiri, Y. Muro, T. Takabatake, and S. Kimura (unpublished).
[21] S. Kimura *et al.*, Phys. Rev. B **50**, 1406 (1994).
[22] B. Bucher *et al.*, Phys. Rev. Lett. **72**, 522 (1994).
[23] H. Okamura *et al.*, Phys. Rev. B **58**, R7496 (1998).
[24] M. Matsunami *et al.*, J. Phys. Soc. Jpn. **72**, 2722 (2003).
[25] M. Dressel *et al.*, Physica (Amsterdam) **230–232B**, 1008 (1997).
[26] G. Li *et al.*, Phys. Rev. Lett. **99**, 027404 (2007).
[27] Z.-T. Zhu *et al.*, Phys. Rev. B **65**, 214519 (2002).
[28] A. S. Barker, Jr., B. I. Halperin, and T. M. Rice, Phys. Rev. Lett. **20**, 384 (1968).